Molecular Activation with Low-Intensity CW Infrared Laser Radiation. Multiphoton Dissociation of Ions Derived from Diethyl Ether

D. S. Bomse,[1] R. L. Woodin,[2] and J. L. Beauchamp*

Contribution No. 5932 from the Arthur Amos Noyes Laboratory of Chemical Physics, California Institute of Technology, Pasadena, California 91125.
Received February 20, 1979

Abstract: Multiphoton dissociation of gas-phase ions derived from $(C_2H_5)_2O$, $(C_2D_5)_2O$, and $C_2H_5OC_2D_5$ using low-intensity infrared CO_2 laser radiation is reported. Techniques of ion cyclotron resonance (ICR) spectroscopy are used to store ions, allowing irradiation for up to 2 s with intensities of 1–100 W cm^{-2}. Reasonably uniform irradiation of the stored ions is achieved with an unfocused laser beam facilitating studies of ion photodissociation kinetics. Decay of the ion population is characterized by an induction period followed by exponential decrease in ion abundance. The induction period is inversely proportional to laser irradiance with the product of these quantities yielding a fluence threshold for the reaction studied. Measured energy fluence thresholds and dissociation rate constants are comparable to data derived from pulsed laser experiments. For all ions which photodissociate only the decomposition process of lowest activation energy is observed. Detailed studies of the effects of collisions on the multiphoton dissociation of the proton-bound dimer $[(C_2H_5)_2O]_2H^+$ are reported. Laser-excited ions are deactivated during irradiation by collisions with neutral buffer gases $(C_2H_5)_2O$, i-C_4H_{10}, and SF_6. Deactivation rate constants are approximately 10–20% of calculated collision rate constants. Collisions prior to irradiation are shown to have no effect on dissociation rates. Collision-free dissociation of $[(C_2H_5)_2O]_2H^+$ is first order in photon flux. Photodissociation spectra of $[(C_2H_5)_2O]_2H^+$, $(C_2H_5)_2OH^+$, and $(C_2D_5)_2OD^+$ are reported and compared to the gas-phase infrared absorption spectrum of the corresponding neutral ether. The dissociation of $(C_2H_5)_2OH^+$ is by β-H transfer yielding $C_2H_5OH_2^+$ and C_2H_4. The competitive multiphoton dissociation of $(C_2H_5)(C_2D_5)OH^+$ shows an isotope effect ≥ 6 favoring β-H transfer. This implies that excitation is very much slower than decomposition above threshold energy. Model calculations treating absorption as a sequential (incoherent) process with decreasing cross section and using RRKM theory to calculate dissociation rates show qualitative agreement with experimental results.

Introduction

A reasonable description of infrared multiphoton excitation using megawatt to gigawatt pulsed lasers is now beginning to emerge. It is generally agreed that initial excitation is by resonant absorption of 3–5 infrared photons in one vibrational mode.[3] Typically, at this level of excitation the rates of intramolecular V–V transfer are sufficient to allow rapid energy transfer to other vibrational modes.[4] Subsequent excitation then proceeds through a sequential incoherent absorption process.[3,5] Standard statistical theories[6] accurately model the unimolecular reactions which occur when the internal excitation of a molecule exceeds threshold.[5,7] Key results from megawatt pulsed laser experiments follow: (1) Multiphoton dissociation is observed under collisionless conditions.[8] (2) Decomposition via the lowest energy pathway is always observed, but is not necessarily the exclusive reaction channel.[9] (3) The spectrum obtained by monitoring the probability of dissociation as a function of laser wavelength is shifted to lower energies and broadened relative to the corresponding infrared absorption spectrum.[3,10,11] Where isotopic substitution introduces shifts in the absorption spectrum, multiphoton dissociation is isotopically selective.[3,11,12] (4) Collisionless dissociation probabilities are largely determined by the total laser pulse energy, with only a small dependence on peak power.[13] (5) There appears to be an energy fluence (energy cm^{-2}) threshold below which dissociation does not occur.[8,14] (6) For many systems studied, collisions during the laser pulse decrease the fraction of molecules dissociated yet increase the total number of photons absorbed.[3,15] More recent experiments have uncovered systems where effects such as rotational hole filling and collisional line broadening contribute to enhanced dissociation yields at higher pressures.[16] (7) Multiphoton excitation rates are sufficiently rapid that molecules may absorb as many as ten photons in excess of the thermodynamic threshold prior to reaction, with the average being in the range of one to three photons.[8,17]

Typical energy fluence thresholds for multiphoton dissociation processes are measured to be 0.1–3.0 J cm^{-2}.[8,14] Since the level of multiphoton excitation depends on energy fluence rather than intensity one infers that multiphoton dissociation can be effected using $\sim$1 W cm^{-2} provided that the target molecules are irradiated under collisionless conditions for at least 1 s. This rather stringent criterion can be satisfied in the laboratory using the techniques of ion cyclotron resonance (ICR) spectroscopy. An obvious requirement for the success of such an experiment is that net absorption rates must exceed spontaneous emission rates. Our recent observation of multiphoton dissociation of gas-phase ions using CW laser intensities of less than 100 W cm^{-2} adds an exciting new dimension to the field of multiphoton activation.[18] Thus photodissociation experiments need not be limited to excitation by megawatt pulsed lasers. In the present study we detail our investigations of low-intensity multiphoton dissociation of ions derived from diethyl ether. Effects of bimolecular interactions, varying laser intensity, and laser wavelength on photodissociation probabilities are explored. Infrared photodissociation spectra of gas-phase ions promise to be a source of previously unobtainable ion structural information.

Experimental Section

The theory, techniques, and instrumentation of trapped ion ICR spectroscopy have been previously described in detail.[19] The spectrometer used in this study was built at Caltech and incorporates a 15-in. electromagnet capable of 23.4 kG. A flat ICR cell is utilized, illustrated in Figure 1, in which the upper source plate is replaced with a 92% transmittance mesh to allow irradiation of trapped ions.

All ICR experiments were carried out in the range 10^{-7}–10^{-5} Torr, corresponding to neutral particle densities of 3×10^9 to 3×10^{11} molecules cm^{-3}. Pressure is measured with a Schulz-Phelps type ionization gauge calibrated against an MKS Instruments Baratron Model 90H1-E capacitance manometer. It is expected that absolute pressure determinations are within $\pm$20% using this method, with pressure ratios being somewhat more accurate. Sample mixtures are

0002-7863/79/1501-5503$01.00/0

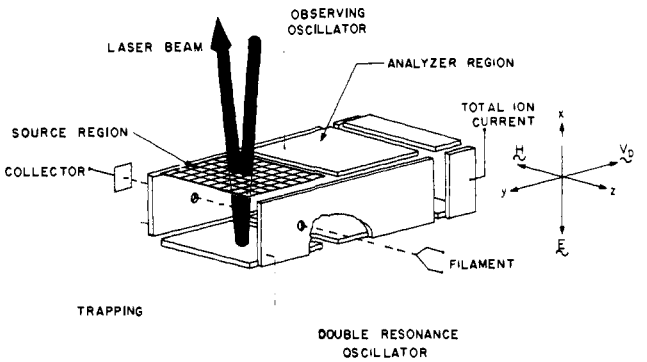

Figure 1. Cutaway view of cyclotron resonance cell. The electron beam is collinear with the magnetic field. The laser beam enters through an open mesh grid comprising the top plate of the source region and is reflected by the lower plate.

prepared directly in the instrument using three sample inlets and the Schulz-Phelps gauge.

Diethyl ether, sulfur hexafluoride, isobutane, and cyclohexane were obtained from commercial sources. Perdeuterated diethyl ether was provided by Professor J. D. Roberts and $C_2H_5OC_2D_5$ was prepared by D. Holtz. All reagents were used without further purification except for the removal of noncondensable gases by several freeze-pump-thaw cycles. Mass spectrometry revealed no detectable impurities. Diethyl ether-d_{10} and $C_2H_5OC_2D_5$ were measured to be >99 and 98.6 atom % pure, respectively.

Gas-phase infrared spectra were obtained using a Perkin-Elmer 257 grating spectrometer. Samples were contained in a 10-cm path length cell equipped with NaCl windows. Wavelength calibration was with polystyrene film.

A schematic view of the experimental apparatus is shown in Figure 2. The laser is an Apollo Model 550A grating tuned CW CO_2 laser. The laser beam profile is nearly Gaussian (fwhm = 6 mm) as determined by measuring the power transmitted through a 1-mm diameter pinhole translated across the beam. Beam shape is monitored with an Optical Engineering Model 22A thermal imaging plate. Infrared laser wavelengths are measured with an Optical Engineering Model 16A spectrum analyzer. Bandwidths are estimated to be 50 MHz. A fraction (25%) of the beam is reflected by a calibrated ZnSe beam splitter (supplied by II-VI Inc.) to a Laser Precision Corp. Model RkP-345 pyroelectric radiometer allowing continuous power measurement. Power fluctuations are typically less than ±5% during an experiment. Maximum stability is achieved by running the laser continuously and controlling irradiation of ions with a Uniblitz Model 225LOA14X5 mechanical shutter. The shutter opening time is measured to be 5 ms.

A turning mirror (Figure 2) directs the beam transverse to the magnetic field into the source region of the ICR cell. The infrared beam enters the vacuum system through an antireflection coated ZnSe window (25.4 mm diameter × 3.5 mm thick) supplied by II-VI, Inc. A mirror finish on the lower source plate (Figure 1) reflects the beam through the source region and out of the apparatus to a graphite beam stop. Assuming that the lower source plate reflects 100% of the incident laser beam and taking into account the 92% mesh transmittance (Figure 1), the beam power inside the cell is 1.84 times the power of the beam entering the vacuum housing. Infrared beam intensities quoted in this paper are calculated by dividing the total power in the beam by the area of the 6-mm diameter beam. Laser intensity in the cell can be varied from 1 to 100 W cm^{-2}. Irradiation of stored ions is uniform as indicated by the fact that small translations of the laser beam do not alter photodissociation rates.

Observed ion decompositions obey first-order kinetics and it is possible to dissociate 100% of the ions. The timing sequence for a typical experiment is illustrated in Figure 3. A 10-ms electron beam pulse generates ions (typically 10^5 ions cm^{-3}) which can be stored for several seconds during which time reactions may occur. The ions are then mass analyzed to determine concentrations of the various species present.[20] Ions of a particular charge to mass ratio can be selectively ejected by ICR double resonance[19] allowing positive identification of reaction pathways. Electronic control of the optical shutter allows the infrared beam to irradiate ions during any portion of the trapping sequence. Ions can be irradiated on alternate trapping cycles and corresponding ion intensities (laser on and laser off) are monitored by a two-channel boxcar integrator. These signals are then processed in a straightforward fashion to yield photodissociation rate constants, even in the presence of ion loss due to diffusion and reaction.[21]

Results and Discussion

A. Ion–Molecule Chemistry of Diethyl Ether. Electron impact ionization of diethyl ether at electron energies greater than 15 eV results in a large variety of fragmentation products. The breakdown diagram shown in Figure 4 illustrates the variation with electron energy of the major ion abundances. Data in Figure 4 are obtained at low pressure and short trapping times to avoid bimolecular reactions. Relative contributions of CHO^+ and $C_2H_5^+$ to the *m/e* 29 signal are ascertained by comparison with the $(C_2D_5)_2O$ breakdown diagram. Similar comparisons indicate that ions observed at *m/e* 43 are due exclusively to $C_2H_3O^+$.

Ion–molecule reactions which occur in diethyl ether involve proton transfer, hydride abstraction, and bimolecular clustering.[22] Proton transfer from fragment ions and parent cation to diethyl ether results in formation of $(C_2H_5)_2OH^+$

$$RH^+ + (C_2H_5)_2O \rightarrow (C_2H_5)_2OH^+ + R \qquad (1)$$

where RH^+ includes $C_2H_3^+$, $C_2H_5^+$, CHO^+, CH_2OH^+, $C_2H_3O^+$, $C_2H_3O^+$, $C_2H_7O^+$, and $C_4H_{10}O^+$. In some cases proton transfer is sufficiently exothermic to induce fragmentation of protonated ether yielding protonated ethanol

$$RH^+ + (C_2H_5)_2O \rightarrow [(C_2H_5)_2OH^+]^* + R \qquad (2a)$$

$$[(C_2H_5)_2OH^+]^* \rightarrow C_2H_5OH_2^+ + C_2H_4 \qquad (2b)$$

where RH^+ includes $C_2H_3^+$, $C_2H_5^+$, and CHO^+. These reactions are confirmed by ICR double resonance.

At pressures greater than 5×10^{-7} Torr and for trapping times greater than 0.5 s $(C_2H_5)_2OH^+$ is observed to react with

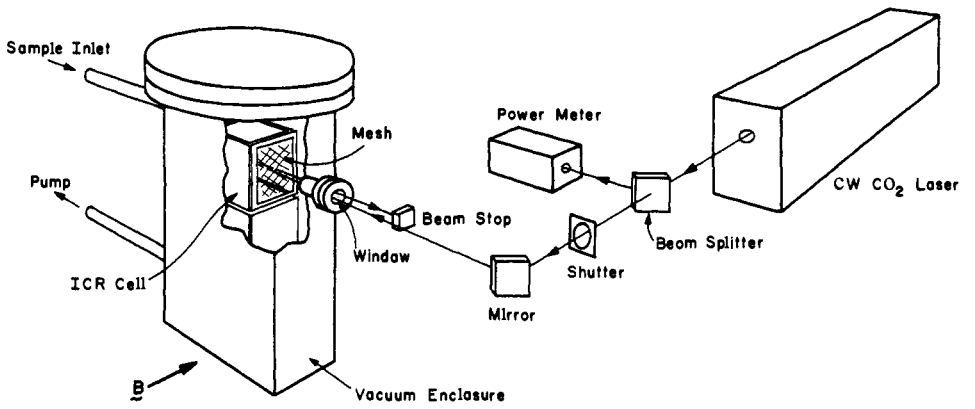

Figure 2. Schematic view of the experimental apparatus.

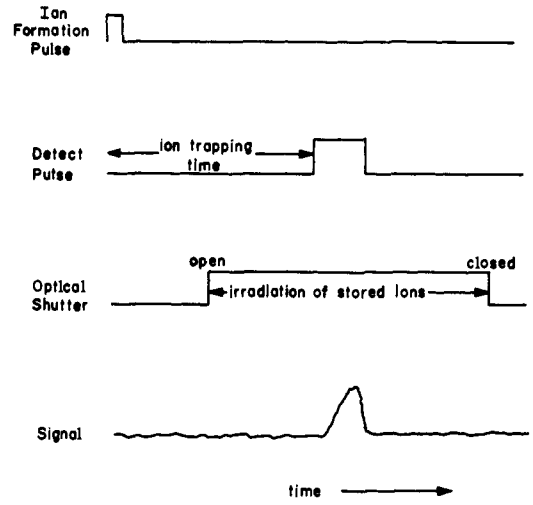

Figure 3. Timing sequence for trapped ion ICR photodissociation experiments. Ions may be irradiated during any portion of the trapping period.

diethyl ether to produce the proton-bound dimer of diethyl ether:

$$(C_2H_5)_2OH^+ + (C_2H_5)_2O \rightarrow [(C_2H_5)_2O]_2H^+ \quad (3)$$

The rate of proton-bound dimer formation measured at three pressures indicated that process 3 is bimolecular with a rate constant of 1.7×10^{-11} cm^3 molecule^{-1} s^{-1}. The rate constant for formation of $[(C_2H_5)_2O]_2H^+$ is obtained from data such as shown in Figure 5, which displays the temporal variation of major ion abundances at a diethyl ether pressure of 4.9×10^{-7} Torr and ionizing energy of 14 eV. Also shown are the data for the hydride abstraction reaction

$$CH_2OC_2H_5^+ + (C_2H_5)_2O \rightarrow CH_3CHOC_2H_5^+ + CH_3OC_2H_5 \quad (4)$$

The measured rate for this reaction is 3.3×10^{-10} cm^3 molecule^{-1} s^{-1}. Not shown in Figure 5 is another hydride abstraction:

$$C_3H_5^+ + (C_2H_5)_2O \rightarrow CH_3CHOC_2H_5^+ + C_3H_6 \quad (5)$$

which gives rise to only a minor fraction (<10%) of the $CH_3CHOC_2H_5^+$ abundance.

As reported previously,[18] both $(C_2H_5)_2OH^+$ and $[(C_2H_5)_2O]_2H^+$ undergo multiphoton dissociation on a time scale such that collisions may deactivate vibrationally excited species. For $(C_2H_5)_2OH^+$ the most obvious deactivation process is symmetric proton transfer.[23] The use of isotopically labeled ether allows detection of symmetric proton transfer:

$$(C_2H_5)_2OH^+ + (C_2D_5)_2O \rightarrow (C_2H_5)_2O + (C_2D_5)_2OH^+ \quad (6)$$

Double resonance ejection of $(C_2D_5)_2OH^+$ prevents the reverse of reaction 6 and leads to exponential decay of $(C_2H_5)_2OH^+$ at a rate equal to the proton-transfer rate. This is determined to be 3.9×10^{-10} cm^3 molecule^{-1} s^{-1}. Similarly, symmetric ether exchange is a possible route for deactivation of laser excited $[(C_2H_5)_2O]_2H^+$ Again, the rate can be measured using a mixture of diethyl ether and diethyl ether-d_{10}. For the reaction

$$[(C_2H_5)_2O]_2H^+ + (C_2D_5)_2O \rightarrow [(C_2H_5)_2O][(C_2D_5)_2O]H^+ + (C_2H_5)_2O \quad (7)$$

the rate constant is 5.3×10^{-12} cm^3 molecule^{-1}s^{-1}, which corresponds to approximately one exchange for every 200 ion-molecule collisions.[24]

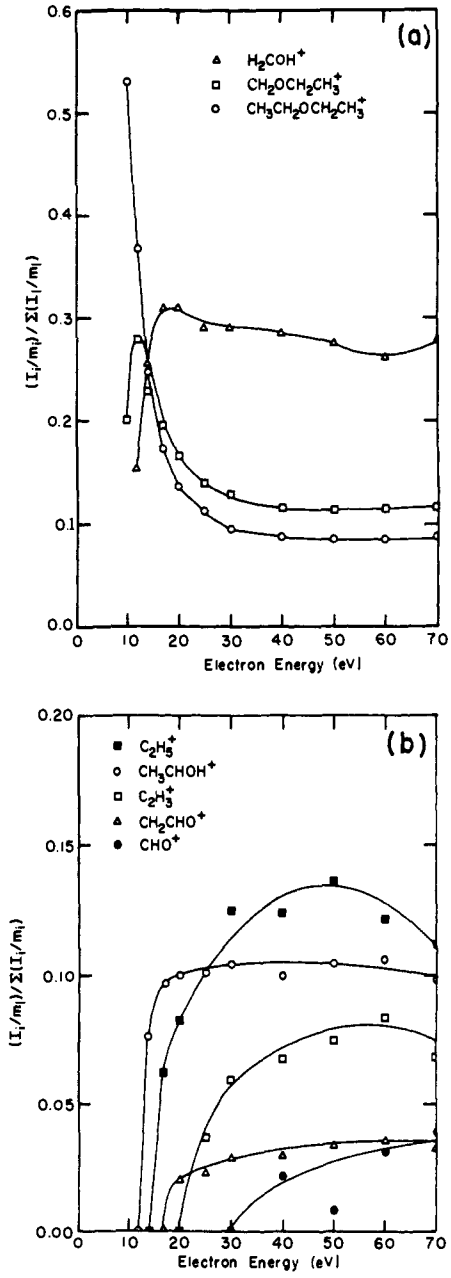

Figure 4. Variation of ion abundance with ionization energy for diethyl ether. Diethyl ether pressure is 6×10^{-7} Torr. (a) Major ions. (b) Minor ions.

B. Infrared Laser Photochemistry of $[(C_2H_5)_2O]_2H^+$. Although infrared absorption bands for ions derived from diethyl ether are unknown, multiphoton dissociation of species such as $[(C_2H_5)_2O]_2H^+$ was anticipated based on strong absorption bands of $(C_2H_5)_2O$ in the 900–1100-cm^{-1} region.[25] Under infrared laser irradiation the proton-bound dimer of diethyl ether is observed to dissociate:[18]

$$[(C_2H_5)_2O]_2H^+ \rightarrow (C_2H_5)_2OH^+ + (C_2H_5)_2O \quad (8)$$

This dissociation reaction is estimated to be 31 ± 2 kcal/mol endothermic, corresponding to absorption of at least 12 photons at the laser wavelengths used.[26] Rupture of the hydrogen bond is not expected to have an activation energy in excess of the reaction endothermicity. At laser intensities sufficient to decompose $[(C_2H_5)_2O]_2H^+$, no dissociation of $(C_2H_5)_2OH^+$ is observed and the increase in abundance of $(C_2H_5)_2OH^+$ exactly matches the decrease in abundance of $[(C_2H_5)_2O]_2H^+$, verifying eq 8 as the only decomposition pathway.

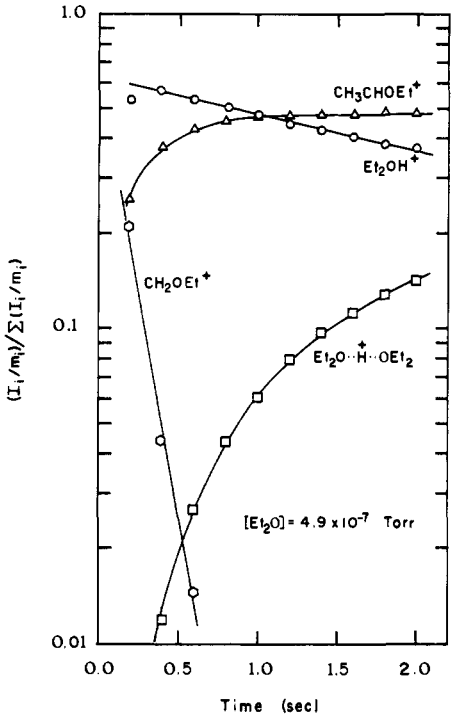

Figure 5. Variation of ion abundance with trapping time for the major ions derived from diethyl ether. Ions are produced by a 10-ms 14-eV electron beam pulse.

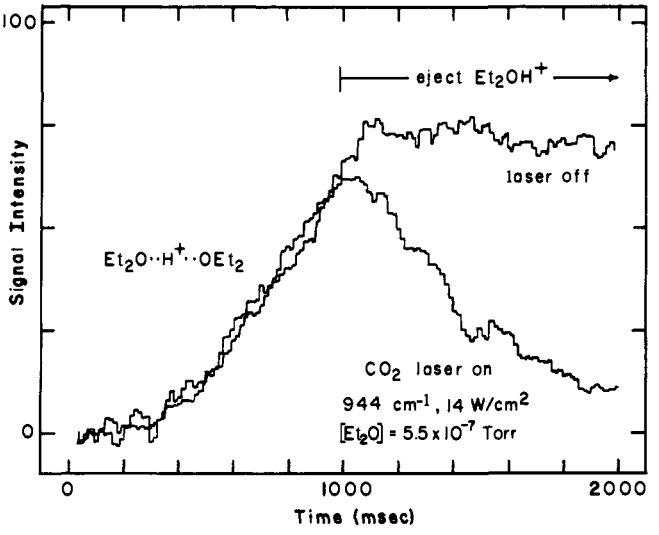

Figure 6. Ion abundance vs. trapping time for a typical multiphoton dissociation experiment. Ions are formed by a 10-ms 70-eV electron beam pulse. The upper trace is the proton-bound dimer signal with the laser off. Ejection of $(C_2H_5)_2OH^+$ beginning at 1-s trapping time halts further dimer formation. CW irradiation by the infrared laser at 14 W cm^{-2} coincident with ejection of $(C_2H_5)_2OH^+$ (lower trace) results in photodissociation of the dimer.

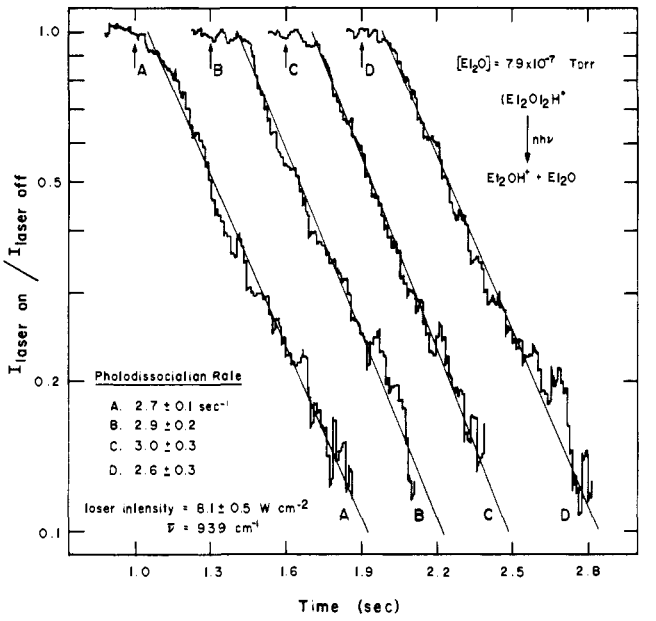

Figure 7. Semilogarithmic plot of fractional ion abundance vs. trapping time for multiphoton dissociation of $[(C_2H_5)_2O]_2H^+$. Data labeled A, B, C, and D are for increasing delays of 0, 300, 600, and 900 ms prior to irradiation. Double resonance ejection of $(C_2H_5)_2OH^+$ begins at 1 s of trapping time. Ions are formed by a 10-ms 14-eV electron beam pulse.

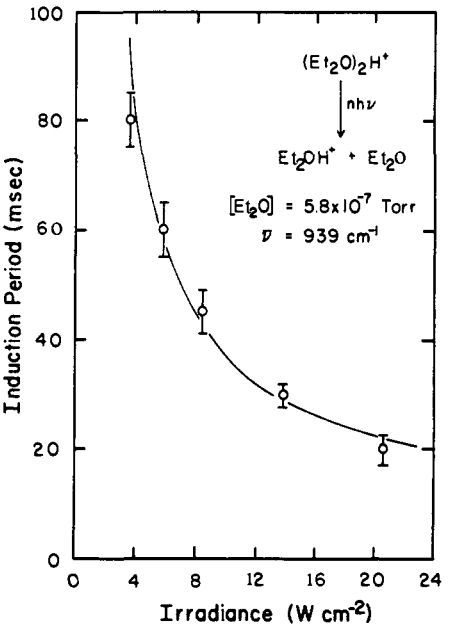

Figure 8. Induction period (defined in text) for multiphoton dissociation of $[(C_2H_5)_2O]_2H^+$ as a function of laser intensity. Ions are formed by a 10-ms 14-eV electron beam pulse. The timing sequence is the same as for Figure 6. The solid line is a plot of eq 9, corrected for the 5-ms shutter opening time.

A typical experiment monitoring $[(C_2H_5)_2O]_2H^+$ is shown in Figure 6. Ions are produced by a 10-ms electron beam pulse and stored for up to 2 s. At 1 s of trapping time the remaining $(C_2H_5)_2OH^+$ is ejected by ICR double resonance in a time short compared with the time between collisions, thus preventing further formation of the dimer, process 3. This is evidenced (Figure 6, upper trace) by the constant abundance of $[(C_2H_5)_2O]_2H^+$ after 1 s. The laser, tuned to 944 cm^{-1}, is gated on at 1 s of trapping time coincident with ejection of $(C_2H_5)_2OH^+$ and effects an exponential decay of the dimer (Figure 6, lower trace).

For data such as presented in Figure 6, the dissociation kinetics are characterized by an induction period followed by an exponential (first-order) decay of the irradiated species. These two features are evident in Figure 7, which shows the logarithm of fractional ion abundance as a function of trapping time with laser irradiation commencing at 1.0, 1.3, 1.6, and 1.9 s, respectively. In all cases double resonance ejection of $(C_2H_5)_2OH^+$ commences at 1.0 s.

The induction period is defined as the time between the shutter opening (vertical arrows in Figure 7) and first observable dissociation. The variation of induction period with

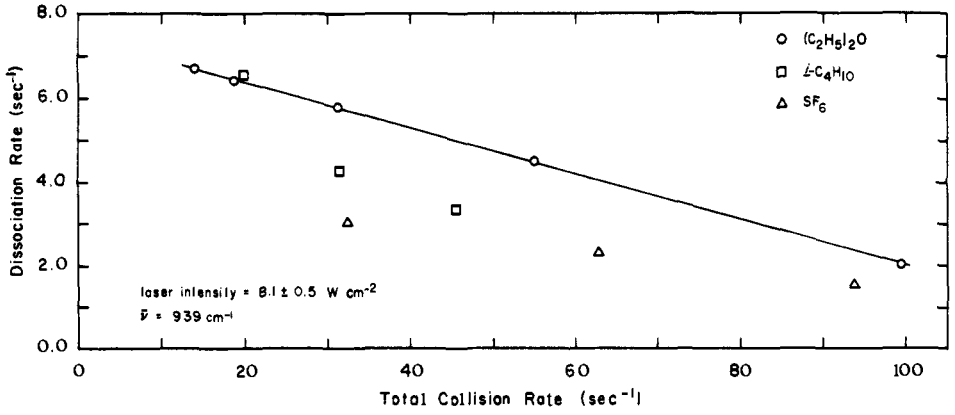

Figure 9. $[(C_2H_5)_2O]_2H^+$ multiphoton dissociation rate as a function of added buffer gases $(C_2H_5)_2O$, SF_6, and i-C_4H_{10}. Dissociation rate is plotted as a function of total collision rate[27] [$(C_2H_5)_2O$ plus buffer gas] to allow direct comparison efficiencies. SF_6 and i-C_4H_{10} are added to 3.7×10^{-7} Torr of diethyl ether. Ionization energy is 14 eV.

laser irradiance is illustrated in Figure 8 for $[(C_2H_5)_2O]_2H^+$ at constant ether pressure. When corrected for a shutter opening time of 5 ms, the data in Figure 8 fit the equation

$$(\text{induction period}) \times I_{las} = 0.3 \text{ J cm}^{-2} \qquad (9)$$

closely (solid line in Figure 8), where I_{las} is the laser irradiance in W cm^{-2}. Equation 9 indicates an energy fluence threshold of 0.3 J cm^{-2} for the observed multiphoton dissociation.

Collisional effects both prior to and during irradiation have been studied in the decomposition of $[(C_2H_5)_2O]_2H^+$. Data in Figure 9 show that photodissociation rate constants decrease with increasing pressure at constant laser intensity, which is the expected effect of collisional deactivation processes. In addition to diethyl ether, results obtained by adding the buffer gases SF_6 and i-C_4H_{10} to a small amount (3.7×10^{-7} Torr) of $(C_2H_5)_2O$ are included in Figure 9. To allow direct comparison of deactivation efficiencies of the three gases, dissociation rates are plotted as a function of ion-molecule collision frequency.[27] For SF_6 and i-C_4H_{10} data points, the limit of zero added buffer gas is defined by the collision rate with the diethyl ether which is present and not by zero collisions. In diethyl ether alone collision rates ten times the dissociation rate reduce the latter by roughly a factor of 2. For a comparable reduction in dissociation rate, collisions with isobutane and SF_6 are respectively 1.5 and 2.5 times as effective as diethyl ether. Thus vibrationally excited ions are quenched by encounters with buffer gas molecules, probably through intermolecular V-V transfer. In the special case where diethyl ether is used as the collision partner, symmetric ether exchange with the proton-bound dimer (eq 7) is too slow to account for the observed deactivation efficiency. It is possible to obtain information regarding the collision-free photodissociation of $[(C_2H_5)_2O]_2H^+$ by extrapolating the data to a low-pressure limit. Here the low-pressure limit is defined by requiring the time between collisions to be long compared with the time for excitation and dissociation of an irradiated ion. The latter is the induction period at the particular laser intensity used. Data, such as shown in Figure 9, were obtained at four different laser powers (1-4 W cm^{-2}). A low-pressure dissociation rate was obtained for each laser power. Figure 10 shows the logarithm of the low-pressure rates as a function of the logarithm of irradiance. Within experimental error the points lie on a straight line of unit slope, implying that $[(C_2H_5)_2O]_2H^+$ photodissociation rate is first order in photon flux. At the low-pressure limit, the equation

$$k = \sigma_D \Phi \qquad (10)$$

relates the dissociation rate k to a phenomenologically defined

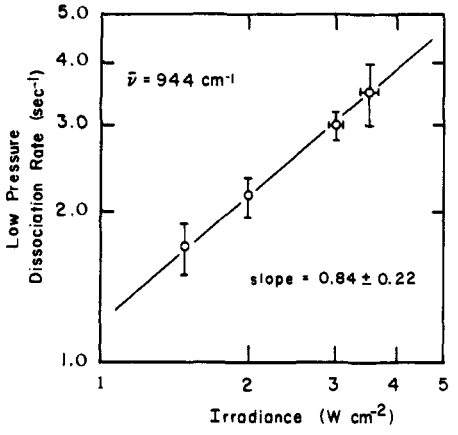

Figure 10. Log-log plot indicating the dependence of $[(C_2H_5)_2O]_2H^+$ low-pressure photodissociation rate on the first power of laser intensity.

cross section, σ_D, and photon flux Φ. The measured cross section at 944 cm^{-1} is $\sigma_D = 2.0 \pm 0.5 \times 10^{-20}$ cm^2.

Since formation of $[(C_2H_5)_2O]_2H^+$ is bimolecular (eq 3) and exothermic the proton-bound dimer may contain up to 31 kcal/mol of internal energy prior to laser photolysis. To probe the effects of vibrational excitation preceding photolyses, an experiment similar to the one depicted in Figure 6 was carried out, modified such that the irradiation was delayed following onset of $(C_2H_5)_2OH^+$ ejection for up to 900 ms. Some of the results from this experiment are presented in Figure 7. Within experimental error, the four multiphoton dissociation rates are identical as are the observed induction periods. For all buffer gas [$(C_2H_5)_2O$, SF_6, and i-C_4H_{10}] pressures up to 4×10^{-6} Torr no change in $[(C_2H_5)_2O]_2H^+$ induction period or photodissociation rate is observed with increasing laser delay. The anticipated effect of vibrational excitation in ions prior to irradiation is an enhanced dissociation rate once irradiation commences. Collisions prior to excitation have no effect on $[(C_2H_5)_2O]_2H^+$ dissociation rates (Figure 7), in contrast to the effect of collisions during irradiation (Figure 9), which inhibit excitation. The invariance of dissociation rate with delay of excitation is surprising. One possible explanation is that the rate of multiphoton excitation of $[(C_2H_5)_2O]_2H^+$ is independent of vibrational energy content of the ion. This is unlikely in view of the fact that vibrationally excited species generally exhibit enhanced multiphoton excitation and dissociation probabilities.[8,28] Given this, the observation of a single decay time in Figure 7 suggest that the system does not behave as if characterized by a broad range of internal energies. Thus, for the experiments in Figure 7, the ions remain

vibrationally excited for times being compared to 900 ms or they have thermalized rapidly, compared to even the shortest delay times prior to irradiation. The latter is more likely since $[(C_2H_5)_2H^+$ ions are formed continuously prior to ejection of $(C_2H_5)_2OH^+$ at 1 s. Thus the proton-bound dimer population reaches half its maximum value at ~700 ms of trapping time (Figure 6) allowing time for radiative and collisional cooling for many of the ions before irradiation.

All three neutral buffer gases show some absorption at the laser wavelength used. Other experiments in this laboratory have demonstrated that irradiation of neutrals at wavelengths corresponding to absorption maxima has no effect on the multiphoton dissociation rates of trapped ions.[28] Calculations of maximum excitation rates by this process indicate that this phenomenon is unimportant under the conditions of our experiments.

The ability to photodissociate the entire $[(C_2H_5)_2O]_2H^+$ population (Figure 6) at even the lowest pressures (corresponding to ~10 collisions s^{-1}) and a fixed wavelength implies that all ions absorb energy at this wavelength.[29] This is consistent with a homogeneously broadened band which may be the result of multiple overlapping vibrational transitions (see below) or broadening due to rapid intramolecular V-V transfer.[4]

C. Infrared Laser Photochemistry of $(C_2H_5)_2OH^+$, $(C_2D_5)_2OD^+$, and $(C_2H_5)(C_2D_5)OH^+$. At low pressures, where proton-bound dimer formation is not significant, multiphoton dissociation of the protonated ether can be studied. The laser-induced process and postulated four-center intermediate[30] are shown in eq 11.[31] Both direct observation of

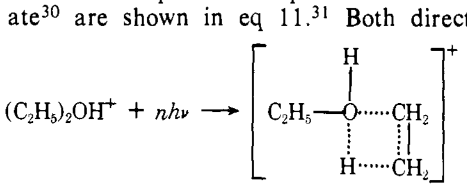

$$\longrightarrow C_2H_5OH_2^+ + C_2H_4 \quad \Delta H = 27 \text{ kcal/mol} \quad (11)$$

$C_2H_5OH_2^+$ formation and ICR double resonance confirm (11) as the reaction pathway. By analogy with similar β-hydrogen transfer processes the activation energy for reaction 11 is expected to be no more than ~2 kcal/mol in excess of the reaction endothermicity.[32] While a less endothermic decomposition route exists,[33] the process

$$(C_2H_5)_2OH^+ + nh\nu \rightarrow CH_3CHOH^+ + C_2H_6 \qquad \Delta H = 15 \text{ kcal/mol} \quad (12)$$

infrared laser photolyses of $(C_2H_5)_2OH^+$ yields exclusively $C_2H_5OH_2^+$. This is consistent with decomposition of vibrationally excited $(C_2H_5)_2OH^+$ formed via exothermic proton transfer (reaction 2) which produces only $C_2H_5OH_2^+$.[22] Thus the activation energy for α-hydrogen transfer to carbon (process 12) must be larger than for β-hydrogen transfer to oxygen (process 11).

Consistent with the results of infrared laser photolyses of $[(C_2H_5)_2O]_2H^+$, photodissociation of $(C_2H_5)_2OH^+$ exhibits an induction period between the start of laser irradiation and the onset of decomposition. Analysis similar to that for $[(C_2H_5)_2O]_2H^+$ (eq 9) indicates that the energy fluence threshold for decomposition of $(C_2H_5)_2OH^+$ is approximately 2 J cm^{-2}. At 944 cm^{-1} the cross section for photodissociation is estimated to be $\sigma_D \simeq 1.0 \times 10^{-21}$ cm^2.

Ions derived from electron impact ionization of $(C_2D_5)_2O$ undergo the identical reactions as do the corresponding unlabeled species. However, with the partially deuterated ether, $C_2H_5OC_2D_5$, an interesting isotope effect is observed in the decomposition of the protonated molecular ion. Chemical ionization of $C_2D_5OC_2H_5$ at low (12 eV) electron energies using cyclohexane as protonating agent allows for selective formation of $(C_2H_5)(C_2D_5)OH^+$ with only trace amounts of $(C_2H_5)(C_2D_5)OD^+$ By analogy with eq 11 there are two possible product ions from the decomposition of $(C_2H_5)(C_2D_5)OH^+$:

$$(C_2H_5)(C_2D_5)OH^+ + nh\nu \rightarrow C_2D_5OH_2^+ + C_2H_4 \quad (13a)$$

$$(C_2H_5)(C_2D_5)OH^+ + nh\nu \rightarrow C_2H_5OHD^+ + C_2D_4 \quad (13b)$$

Yet, during laser irradiation, $C_2D_5OH_2^+$ is the only product detected, irrespective of laser wavelength, process 13a. Thus β-hydrogen transfer in the four-center intermediate is more facile than β-deuterium transfer. Consideration of ion detection limits in this experiment provides a lower limit for the combined primary and secondary isotope effects (defined as the ratio of rates of product ion formation) as $\geqslant 6$. In comparison, when $(C_2H_5)(C_2D_5)OH^+$ is formed by highly exothermic proton transfer (eq 2) such that the protonated ether internal energy greatly exceeds the decomposition threshold, the observed isotope effect is ~2.[34] These results suggest that multiphoton dissociation occurs at an energy only slightly in excess of thermodynamic threshold. Large primary isotope effects have also been reported for metastable ion decompositions which occur at energies near threshold.[35] Thus, the excitation rate must be slow compared to the unimolecular decomposition rate.

The relatively slow time scale for low-intensity infrared laser excitation implies that standard statistical treatments of unimolecular reactions[6] can be utilized to describe the decomposition of multiphoton excited ions. RRKM calculations on $(C_2H_5)(C_2D_5)OH^+$ decomposition indicate that dissociation rates become extremely large ($>10^3$ s^{-1}) within several kilocalories per mole above decomposition threshold, in agreement with the conclusions drawn from experimental results. Figure 11 shows the calculated isotope effect in decomposition of $(C_2H_5)(C_2D_5)OH^+$ as a function of internal energy in excess of threshold. The experimentally measured value of $\geqslant 6$ from infrared photodissociation is consistent with decomposition close to threshold. At higher energies, the isotope effect is ~2, in agreement with the chemical activation experiments. For these calculations, vibrational frequencies are assumed similar to the neutral molecule with appropriate frequencies added involving proton vibration. A tight transition state is assumed, in accordance with standard treatments for four-centered transition states[6,35,36] (eq 11).

As each of the proton-transfer reactions which produce $(C_2H_5)_2OH^+$ (eq 1) is exothermic, the protonated ether may be vibrationally excited in the absence of deactivating collisions. The distribution of internal energies is quite complex because each of the eight proton-transfer reactions imparts a different amount of energy to $(C_2H_5)_2OH^+$. Changing the ionization energy alters the relative abundances of fragment ions (Figure 4) which lead to formation of $(C_2H_5)_2OH^+$ and so varies the internal energy content of the protonated ether. The results of using ionization energies of 14 and 70 eV are shown in Figure 12. Laser irradiation is continuous in this experiment. The increase in photodissociation rate with 70-eV electrons compared to 14-eV electrons, readily apparent in Figure 12, is most likely due to proton-transfer reactions of greater exothermicity at 70 eV. Although symmetric proton transfer, reaction 6, represents an efficient deexcitation process, the low pressures used to study $(C_2H_5)_2OH^+$ limit the total ion-molecule collision rate to less than 15 s^{-1}.[27] Low diethyl ether pressure is necessary to minimize proton-bound dimer formation. Thus vibrationally excited ions are sufficiently long lived to be observed in the multiphoton dissociation process, Figure 12. Quantitative determination of the effects of prior vibrational excitation on $(C_2H_5)_2OH^+$ decomposition were not pursued owing to complications caused by the presence of a multitude of proton-transfer reactions forming

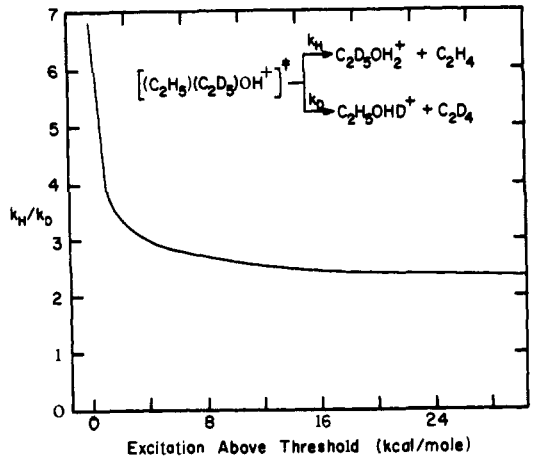

Figure 11. Calculated isotope effect in decomposition of $(C_2H_5)(C_2D_5)$-OH^+ as a function of internal energy in excess of decomposition threshold.

$(C_2H_5)_2OH^+$ and the necessity of accounting for $(C_2H_5)_2OH^+$ formation during irradiation (Figure 12).

D. Infrared Laser Photochemistry of $CH_3CHOC_2H_5^+$, $C_2H_5OH_2^+$, and CH_3CHOH^+. Photodissociation of $CH_3CHOC_2H_5^+$ is observed at laser intensities similar to those required for dissociation of $(C_2H_5)_2OH^+$ [18] ICR double resonance confirms the process

$$CH_3CHOC_2H_5^+ + nh\nu \rightarrow CH_3CHOH^+ + C_2H_4 \qquad \Delta H = 34 \text{ kcal/mol} \quad (14)$$

as the only decomposition pathway,[31] which is also the decomposition of lowest endothermicity. σ_D estimated for this process (λ 944 cm^{-1}) is $\sim 4 \times 10^{-22}$ cm^2. Since reaction 14 involves β-hydrogen transfer in a four-center intermediate similar to process 11, the activation energy is again assumed to be less than ~2 kcal/mol in excess of the reaction endothermicity.

Higher laser intensities than those required for photodissociation of $(C_2H_5)_2OH^+$ or $CH_3CHOC_2H_5^+$ result in decomposition of $C_2H_5OH_2^+$. Of the low-enthalpy dissociation pathways available,[31] reaction 15, the observed process with laser irradiation (confirmed by double resonance) is reaction 15a. This result is consistent with results from decomposition

$$C_2H_5OH_2^+ + nh\nu \rightarrow H_3O^+ + C_2H_4 \qquad \Delta H = 27 \text{ kcal/mol} \quad (15a)$$

$$C_2H_5OH_2^+ + nh\nu \rightarrow CH_3CHOH^+ + H_2 \qquad \Delta H = 21 \text{ kcal/mol} \quad (15b)$$

of chemically activated $C_2H_5OH_2^+$.[37] While reaction 15b has a lower ΔH, chemical ionization studies of protonated methanol decomposition indicate a barrier of approximately 1 eV in excess of the reaction endothermicity for hydrogen elimination, and no activation energy above the endothermicity for loss of H_3O^+.[37] The observed laser-induced photodissociation process is thus the decomposition of lowest activation energy.[38] σ_D for infrared multiphoton dissociation of $C_2H_5OH_2^+$ at 944 cm^{-1} is $\sim 1 \times 10^{-22}$ cm^2. No dissociation of CH_3CHOH^+ is observed with infrared laser radiation in the 900–1100-cm^{-1} region.

E. Photodissociation Spectra. For all systems studied the photodissociation products are invariant to change in laser wavelength. The wavelength dependences for multiphoton dissociation probabilities of $(C_2H_5)_2OH^+$ and $[(C_2H_5)_2O]_2H^+$ are shown in Figure 13a and data for $(C_2D_5)_2OD^+$ are shown in Figure 13b. Also shown are the gas-phase absorption spectra of the corresponding neutrals over the range of CO_2 laser wavelengths (note the change of scale in the axes for percent transmission). P_D is defined as the fractional dissociation yield

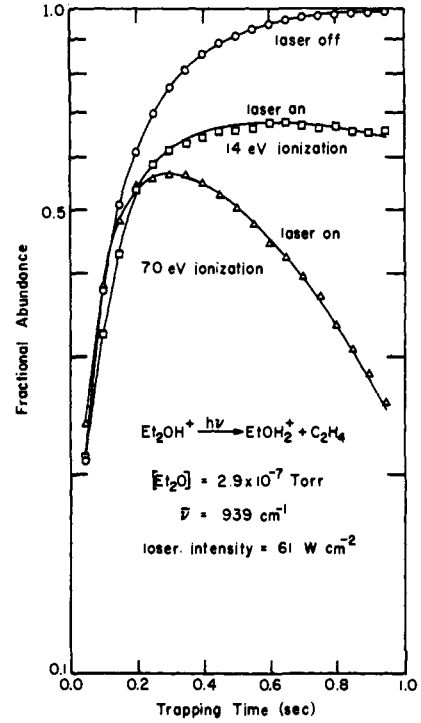

Figure 12. Fractional ion abundance vs. trapping time for multiphoton dissociation of $(C_2H_5)_2OH^+$. Data is shown for laser off conditions, and laser on conditions where the ionization energies are 14 and 70 eV. The laser off curve is the same for both 14 and 70 eV ionization energies. Laser irradiation is continuous beginning at $t = 0$ s.

for a particular irradiation time and laser intensity. For both $(C_2H_5)_2OH^+$ and $(C_2D_5)_2OD^+$ experimental conditions are nearly identical. Differences in P_D values for the monomer species are thus a direct measure of differences in cross sections for multiphoton dissociation at each wavelength. No such direct comparison regarding dissociation cross sections can be made between the protonated ether and the proton-bound dimer owing to differences in laser intensity and ether pressure for the two experiments.

Analysis of the infrared photodissociation spectra (Figures 13a,b) rests on the assumption that multiphoton dissociation spectra somewhat mimic small signal absorption spectra, as is observed in infrared laser photolyses of neutrals.[3,10,11] Observed bands in the infrared spectrum of diethyl ether from 900 to 1100 cm^{-1} are assigned to combinations of C-C stretches, C-O stretches, and methylene wags.[25] Protonation of the ether should not significantly affect the C-C stretch and methylene wag frequencies. It is seen in Figure 13a that the $(C_2H_5)_2OH^+$ photodissociation spectrum exhibits local maxima at roughly the same wavelengths as the diethyl ether absorption spectrum. Vibrational frequencies of protonated ether and the proton-bound dimer are expected to be similar with the exception of low frequency skeletal torsions and vibrations associated with proton motion. Neither of these special cases is expected to involve vibration in the 900–1100-cm^{-1} region excited in photodissociation experiments. Thus the photodissociation spectra of $(C_2H_5)_2OH^+$ and $[(C_2H_5)_2O]_2H^+$ show nearly identical maxima.

Theoretical Implications

While it is tempting to apply current theories for megawatt pulsed laser multiphoton dissociation[3,5,7,39a-i] to low-intensity infrared photolyses of gas-phase ions, there are inherent differences between the two types of experiments which necessitate modification of the existing developed theories. In particular, the time scale of the ICR experiments requires consideration of spontaneous emission (typically 1–100 s^{-1} [40]) as

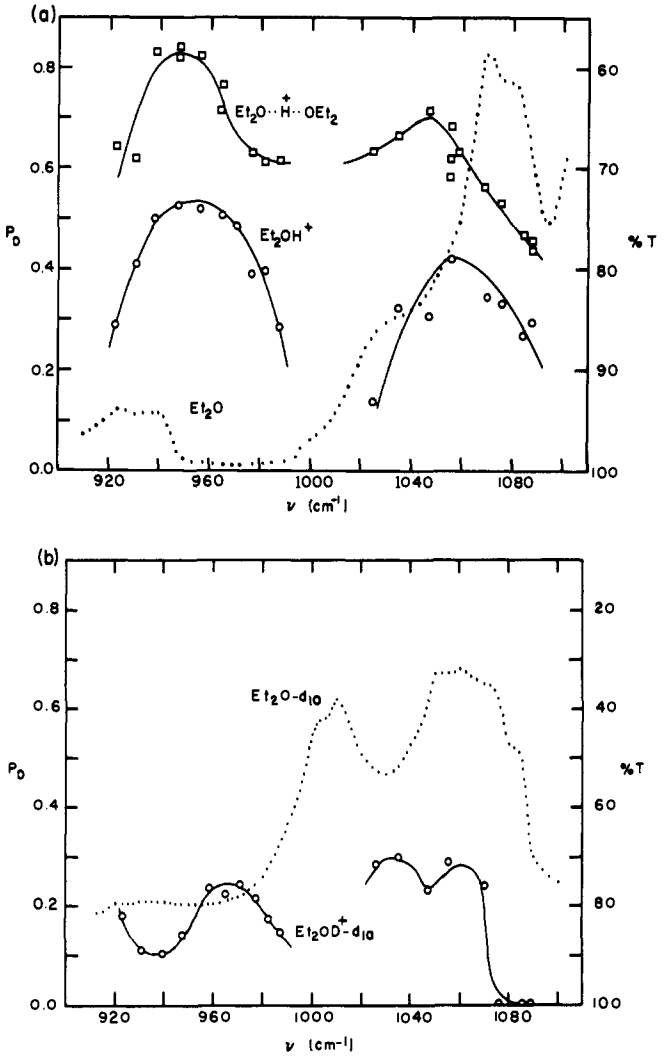

Figure 13. (a) Photodissociation spectra of $(C_2H_5)_2OH^+$ and $[(C_2H_5)_2O]_2H^+$ over the CO_2 laser spectral range. For $(C_2H_5)_2OH^+$, P_D is the fraction of ions dissociated after 1.9 s of irradiation at 48 W cm^{-2}; $(C_2H_5)_2O$ pressure is 8.8×10^{-8} Torr. P_D for $[(C_2H_5)_2O]_2H^+$ is defined as the fraction of ions dissociated after 2.0 s of irradiation at 10 W cm^{-2}; $(C_2H_5)_2O$ pressure is 4.7×10^{-7} Torr. Ionization energy for both experiments is 14 eV. Dotted line is the infrared absorption spectrum of diethyl ether at 20 Torr. (b) Photodissociation spectrum of $(C_2D_5)_2OD^+$ over the CO_2 laser spectral range. Experimental conditions are the same as for photodissociation of $(C_2H_5)_2OH^+$ in (a). Dotted line is the infrared absorption spectrum of $(C_2D_5)_2O$ at 16 Torr.

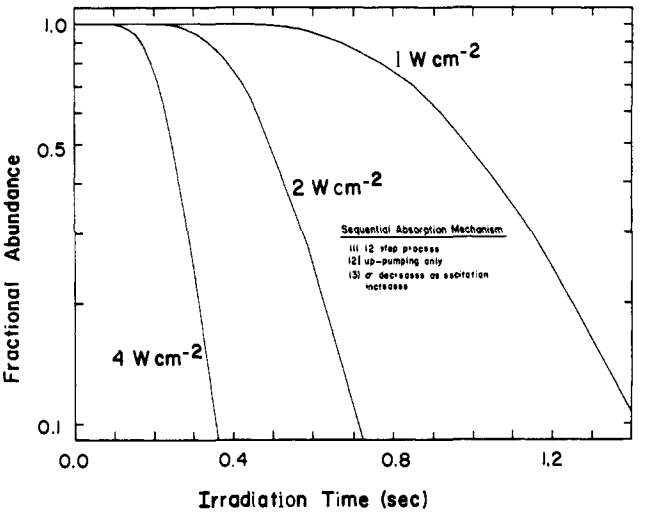

Figure 14. Model calculations of slow multiphoton dissociation. The calculation follows Scheme I, assuming $n = 12$ and only excitation processes are involved. The form of the absorption cross section at each level of excitation is given by eq 16.

a viable deactivation mechanism. Equally important, the low laser intensities obviate power broadening[41] as a mechanism for overcoming anharmonicities in hot band absorptions.

Several authors point out that at high levels of internal excitation vibrational state densities become large, guaranteeing the availability of at least one vibrational state within the laser bandwidth.[3] This defines the quasi-continuum of vibrational states. Theories of excitation through the quasi-continuum treat the process as a sequence of incoherent single-photon absorptions.[5,7,8,14,39c] Model calculations[5] of sequential absorption through the quasi-continuum using cross sections obtained from photoacoustic spectra[7] agree well with pulsed laser multiphoton dissociation yields.

If absorption through the quasi-continuum is facile due to the availability of resonant transitions, then the ability to photodissociate a molecule with low-intensity radiation depends on the ease of populating the quasi-continuum. Molecules in which the quasi-continuum is attained by absorption of a single photon are expected to photodissociate most readily, while molecules requiring absorption of two or more photons should, in the absence of power broadening, be much more difficult to photodissociate. Molecules possessing many degrees of freedom will have a significant amount of internal energy at ambient temperature.[29] The combination of many vibrational modes and appreciable thermal energy content serves to locate such molecules very nearly in the quasi-continuum prior to laser excitation. Although not all vibrational frequencies of $[(C_2H_5)_2O]_2H^+$ and $(C_2H_5)_2OH^+$ are known, approximating the frequencies with those reported for diethyl ether[25] permits an estimate of the density of vibrational states in the ions. Using the well-known Whitten-Rabinovitch approximation,[6] the densities of states in $[(C_2H_5)_2O]_2H^+$ at energies corresponding to absorption of one and two infrared photons (1000 cm^{-1}) are 120 and 9×10^4 states/cm^{-1}, respectively. The CW CO_2 laser bandwidth of $\sim$0.001 cm^{-1} implies that for the proton-bound dimer, the quasi-continuum is accessible following the resonant absorption of a single infrared photon. In comparison, the estimated densities of states in $(C_2H_5)_2OH^+$ corresponding to absorption of one and two infrared photons are 2 and 94 states/cm^{-1}. For the protonated ether, the quasi-continuum is not reached until the absorption of four infrared photons (density of states $\simeq 2 \times 10^4$ states/cm^{-1}) occurs. These arguments concerning the densities of states in the ions explain why multiphoton dissociation of $[(C_2H_5)_2O]_2H^+$ is facile while decomposition of $(C_2H_5)_2OH^+$ requires considerably higher laser powers. In fact, at room temperature, the proton-bound dimer contains 3-4 kcal/mol internal energy in excess of the zero-point energy due to thermal population of vibrational states. This energy is comparable to excitation by a single infrared photon. The availability of many overlapping vibrational transitions allows all ions to absorb over a wide range of frequencies. Dissociation of the entire population is thus possible even under collisionless conditions.

If in fact the proton-bound dimer is very nearly in the quasi-continuum prior to excitation then the same analysis used for pulsed laser model calculations[5] should apply to low-intensity photolyses with allowances made for deactivation due to spontaneous emission. Applying eq 9 to megawatt powers and short pulse duration predicts induction periods commensurate with the pulsed laser model calculations mentioned above. In a complementary fashion, scaling the model calculations[5] to low laser intensities yields results very similar to experimentally observed multiphoton dissociation reactions with CW radiation. Scheme I illustrates the sequential

Scheme I

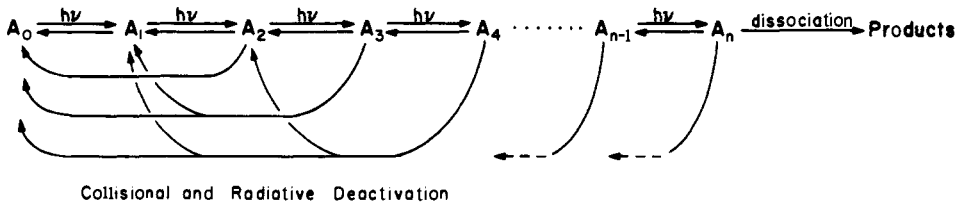

mechanisms assumed for low-intensity infrared multiphoton dissociation, where both collisions and spontaneous emission are deactivation processes. Assuming that absorption cross sections are similar to those derived for SF_6, preliminary model calculations following Scheme I and including only excitation processes are shown in Figure 14. The form for the absorption cross section used in given in the equation[8]

$$\sigma(n) = \exp(-42.9 - 0.029n)\ \text{cm}^2 \qquad (16)$$

where n is the number of photons absorbed. The calculation in Figure 14 assumes 12 excitation steps (corresponding to the number of photons required for dissociation of $[(C_2H_5)_2O]_2H^+$) and that dissociation is rapid compared to excitation above threshold. Calculation of decomposition rates near threshold indicates rates which are rapid compared to the excitation rates ($<50\ s^{-1}$) used in the model. It is apparent from Figure 14 that, even though the calculation uses data for SF_6 and includes only excitation, both the induction period and decomposition rates agree qualitatively with experimental data, Figure 7. However, the calculated induction periods are considerably longer than experimentally determined values and the calculated decays show more curvature than is observed. The preliminary calculation serves to illustrate the utility of the model and inclusion of more realistic cross sections in addition to deactivation processes should allow reasonable modeling of the low-intensity photolyses.

Conclusions

The large temporal and spatial inhomogeneities of the laser field inherent in pulsed laser studies of multiphoton dissociation are avoided by the use of low-intensity unfocused CW radiation. In many respects the present results are similar to pulsed laser experiments. In all cases studied, low-intensity multiphoton dissociation proceeds via the lowest energy pathway, as seen in pulsed laser experiments. However, in low-intensity photolyses dissociation appears to be very nearly at threshold, unlike multiphoton dissociation using pulsed lasers in which excitation may be substantially above the threshold because of the much faster excitation rates. Unlike high-power pulsed laser photodissociation, no appreciable shift to lower energies in the photodissociation spectrum is found with low-intensity excitation. This is likely due to the inherently different nature of initial excitation in the two processes. Whereas pulsed laser experiments rely on power broadening to coherently absorb three to five photons in a single mode (and hence exhibit a spectral shift to lower energy because of anharmonicity effects), the low-intensity excitation precludes power broadening and the photodissociation spectrum is expected to be similar to the ground-state spectrum. Isotopic substitution resulting in shifts of bands in absorption spectra is expected to allow isotopic selectivity in slow multiphoton dissociation. In the case of $[(C_2H_5)_2O]_2H^+$ a single resonant absorption may populate the vibrational quasi-continuum. However, the mechanism for excitation to the quasi-continuum in $(C_2H_5)_2OH^+$, $CH_3CHOC_2H_5^+$, and $C_2H_5OH_2^+$ is not obvious. In agreement with pulsed laser experiments, low-intensity multiphoton dissociation yields are proportional to energy fluence and an energy fluence threshold is observed. The magnitudes of the energy fluence threshold and photodissociation cross section for $[(C_2H_5)_2O]_2H^+$ measured in the low-intensity experiment ($0.3\ \text{J cm}^{-2}$ and $2 \times 10^{-20}\ \text{cm}^2$, respectively) are similar in magnitude to those measured for SF_6 in pulsed laser experiments ($1.4\ \text{J cm}^{-2}$ [14] and $1.5 \times 10^{-20}\ \text{cm}^2$,[8] respectively). For ions derived from diethyl ether the effect of collisions during low-intensity irradiation is only to deactivate excited species, as observed in high-intensity pulsed experiments.

There are many possible extensions and applications of the present work. Collisional and radiative relaxation mechanisms can be probed in great detail by observing their effect on multiphoton dissociation. Low-intensity multiphoton dissociation provides a convenient method for obtaining hitherto unknown vibrational spectra of gas-phase ions. The availability of CO, hydrogen halide, optically pumped far-infrared lasers, F-center lasers, and optically pumped parametric oscillators will extend the spectral range beyond the 9–11-μm region. Photodissociation spectra should allow differentiation among structural isomers of ions.

Acknowledgment. This work was supported in part by the U.S. Department of Energy and the President's Fund of the California Institute of Technology.

References and Notes

(1) NSF Predoctoral Fellow, 1976–1979.
(2) Exxon Research and Engineering Co., Corporate Research Laboratories, Linden, N.J. 07036.
(3) R. V. Ambartzumian and V. S. Letokhov in "Chemical and Biochemical Applications of Lasers", Vol. III, C. Bradley Moore, Ed., Academic Press, New York, 1977, and references cited therein.
(4) H. S. Kwok and E. Yablonovitch, *Phys. Rev. Lett.*, **41**, 745 (1978); D. S. Frankel, Jr., and T. J. Manuccia, *Chem. Phys. Lett.*, **54**, 451 (1978).
(5) E. R. Grant, P. A. Schulz, Aa. S. Sudbo, Y. R. Shen, and Y. T. Lee, *Phys. Rev. Lett.*, **40**, 115 (1978).
(6) P. J. Robinson and K. A. Holbrook, "Unimolecular Reactions", Wiley-Interscience, New York, 1972.
(7) J. G. Black, E. Yablonovitch, N. Bloembergen, and S. Mukamel, *Phys. Rev. Lett.*, **38**, 1131 (1977); M. J. Shultz and E. Yablonovitch, *J. Chem. Phys.*, **68**, 3007 (1978).
(8) M. J. Coggiola, P. A. Schulz, Y. T. Lee, and Y. R. Shen, *Phys. Rev. Lett.*, **38**, 17 (1977); E. R. Grant, P. A. Schulz, Aa. S. Sudbo, M. J. Coggiola, Y. R. Shen, and Y. T. Lee, Proceedings of the International Conference on Multiphoton Processes, Rochester, N.Y., J. H. Eberly and P. Lambropoulos, Eds., Wiley, New York, 1978; Aa. S. Sudbo, P. A. Schulz, E. R. Grant, Y. R. Shen, and Y. T. Lee, *J. Chem. Phys.*, **68**, 1306 (1978).
(9) D. M. Brenner, *Chem. Phys. Lett.*, **57**, 357 (1978); R. N. Rosenfeld, J. I. Brauman, J. R. Barker, and D. M. Golden, *J. Am. Chem. Soc.*, **99**, 8063 (1977).
(10) A. Hartford, Jr., *Chem. Phys. Lett.*, **53**, 503 (1978).
(11) D. S. King and J. C. Stephenson, *J. Am. Chem. Soc.*, **100**, 7151 (1978).
(12) J. J. Tiee and C. Wittig, *Appl. Phys. Lett.*, **32**, 236 (1978).
(13) P. Kolodner, C. Winterfeld, and E. Yablonovitch, *Opt. Commun.*, **20**, 119 (1977).
(14) N. Bloembergen and E. Yablonovitch, "Laser Spectroscopy", Vol. III, J. L. Hall and J. L. Carlsten, Eds., Springer Series in Optical Sciences, Springer-Verlag, West Berlin, 1977.
(15) E. Grunwald, K. J. Olszyna, D. F. Dever, and B. Knishkowy, *J. Am. Chem. Soc.*, **99**, 6515 (1977); G. P. Quigley in "Advances in Laser Chemistry", A. H. Zewail, Ed., Springer Series in Chemical Physics, Springer-Verlag, West Berlin, 1978, and references cited therein.
(16) C. R. Quick and C. Wittig, *J. Chem. Phys.*, **69**, 4201 (1978); J. C. Stephenson, private communication.
(17) A. J. Colussi, S. W. Benson, R. J. Hwang, and J. J. Tiee, *Chem. Phys. Lett.*, **52**, 349 (1977).
(18) R. L. Woodin, D. S. Bomse, and J. L. Beauchamp, *J. Am. Chem. Soc.*, **100**, 3248 (1978).
(19) T. A. Lehman and M. M. Bursey, "Ion Cyclotron Resonance Spectrometry", Wiley-Interscience, New York, 1976; J. L. Beauchamp, *Annu. Rev. Phys. Chem.*, **22**, 527 (1971).
(20) T. B. McMahon and J. L. Beauchamp, *Rev. Sci. Instrum.*, **43**, 509 (1972).
(21) R. L. Woodin, D. S. Bomse, T. B. McMahon, and J. L. Beauchamp, to be published.
(22) J. L. Beauchamp, Ph.D. Thesis, Harvard University, 1967.
(23) T. B. McMahon, P. G. Miasek, and J. L. Beauchamp, *Int. J. Mass Spectrom.*

Ion Phys., 21, 63 (1976).
(24) Ion–molecule collision frequencies are calculated using average dipole orientation theory: L. Bass, T. Su, W. J. Chesnavich, and M. T. Bowers, Chem. Phys. Lett., 34, 119 (1975).
(25) H. Wieser, W. G. Laidlaw, P. J. Krueger, and H. Fuhrer, Spectrochim. Acta, Part A, 24, 1055 (1968); J. P. Perchard, J. C. Monier, and P. Dizabo, Ibid., 27, 447 (1971).
(26) The estimated enthalpy change for reaction 1 is based on measured enthalpy changes for analogous reactions of H_3O^+, $CH_3OH_2^+$, and $(CH_3)_2OH^+$; P. Kebarle, Annu. Rev. Phys. Chem., 28, 445 (1977).
(27) $[(C_2H_5)_2O]_2H^+$ collision rate constants, calculated using ADO theory,[24] are 1.2×10^{-9} cm^3 molecule^{-1} s^{-1} for $(C_2H_5)_2O$, 6.1×10^{-10} cm^3 molecule^{-1} s^{-1} for SF_6, and 1.0×10^{-9} cm^3 molecule^{-1} s^{-1} for i-C_4H_{10}.
(28) R. L. Woodin, D. S. Bomse, and J. L. Beauchamp, Chem. Phys. Lett., 63, 630 (1979).
(29) Similar observations have been made for multiphoton dissociation of bishexafluoroacetylacetonateuranyl–tetrahydrofuran in a molecular beam: A. Kaldor, R. B. Hall, D. M. Cox, J. A. Horsley, P. Rabinowitz, and G. M. Kramer, J. Am. Chem. Soc., submitted.
(30) C. W. Tsang and A. G. Harrison, Org. Mass Spectrom., 3, 647 (1970).
(31) Ion heats of formation obtained from appropriate proton affinity data, neutral heats of formation, and tabulated ion thermochemistry. J. F. Wolf, R. H. Staley, I. Koppel, M. Taagepera, R. T. McIver, Jr., J. L. Beauchamp, and R. W. Taft, J. Am. Chem. Soc., 99, 5417 (1977); H. M. Rosenstock, K. Draxl, B. W. Steiner, and J. T. Herron, J. Phys. Chem. Ref. Data, Suppl. 1, 6, (1977); J. D. Cox and G. Pilcher, "Thermochemistry of Organic and Organometallic Compounds", Academic Press, New York, 1970.
(32) R. Botter, J. M. Pechine, and H. M. Rosenstock, Int. J. Mass Spectrom. Ion Phys., 25, 7 (1977).
(33) Analogous 1, 2 eliminations of H_2 from gas-phase ions have activation energies >80 kcal/mol. D. H. Williams, Acc. Chem. Res., 10, 280 (1977).
(34) D. Holtz and J. L. Beauchamp, unpublished results.
(35) Dudley Williams and George Hvistendahl, J. Am. Chem. Soc., 96, 6753 (1974).
(36) Frequencies in the transition state estimated using bond-order arguments.[6] Frequencies used for proton motion are 3600, 1600, and 500 cm^{-1}.[42] In the transition state, both $-CH_3$ and $-C_2H_5$ rotations are frozen out. All internal rotations are treated as torsions. Activation energies are assumed the same as for process 11, with zero point energy differences due to deuterium substitution taken into account.
(37) W. T. Huntress, Jr., D. K. Sen Sharma, K. R. Jennings, and M. T. Bowers, Int. J. Mass Spectrom. Ion Phys., 24, 25 (1977).
(38) We have erroneously identified the products of this reaction in another publication: R. L. Woodin, D. S. Bomse, and J. L. Beauchamp in "Chemical and Biochemical Applications of Lasers," Vol. IV, C. B. Moore, Ed., Academic Press, New York, 1979.
(39) (a) C. D. Cantrell, S. M. Freund, and J. L. Lyman in "Laser Handbook", Vol. III, North-Holland Publishing Co., Amsterdam, in press; (b) C. D. Cantrell in "Laser Spectroscopy", Vol. III, J. L. Hall and J. L. Carlsten, Eds., Springer Series in Optical Sciences, Springer-Verlag, West Berlin, 1977; (c) N. Bloembergen, Opt. Commun., 15, 416 (1975); (d) M. F. Goodman, J. Stone, and D. A. Dows, J. Chem. Phys., 65, 5052 (1976); (e) S. Mukamel and J. Jortner, Chem. Phys. Lett., 40, 150 (1976); (f) S. Mukamel and J. Jortner, J. Chem. Phys., 65, 5204 (1976); (g) M. Tamir and R. D. Levine, Chem. Phys. Lett., 46, 208 (1977); (h) D. P. Hodgkinson and J. S. Briggs, ibid., 43, 451 (1976); (i) M. Quack, J. Chem. Phys., 69, 1294 (1978).
(40) G. Herzberg, "Infrared and Raman Spectra of Polyatomic Molecules", Van Nostrand, Princeton, N.J., 1945, p 251.
(41) For typical infrared transition moments of 0.01–0.20 D and laser intensity of 1 W cm^{-2}, the Rabi frequency is $\sim 10^5$ s^{-1} corresponding to power broadening of $\ll 0.001$ cm^{-1}.
(42) G. H. F. Diercksen, W. P. Kraemer, and B. O. Roos, Theor. Chim. Acta, 36, 249 (1975).

Thermodynamics of Hydrolysis of Aliphatic Ketals. An Entropy Component of Steric Effects

Kenneth B. Wiberg* and Robert R. Squires

Contribution from the Department of Chemistry, Yale University, New Haven, Connecticut 06520. *Received November 7, 1978*

Abstract: The enthalpies and free energies of the acid-catalyzed hydrolysis of a series of alkyl-substituted dimethyl ketals have been determined in a model study of steric effects. The measured enthalpy differences did not correlate with standard quantitative notions of the steric bulk of the substituents, although the overall free-energy changes fit the expected order. The entropy effect of the substituents is a dominant factor in determining the equilibrium composition for this reaction. Possible origins for these entropy effects are discussed.

Introduction

Steric effects are widely recognized as one of the most important factors which may act to control the course of an organic reaction. Most of the quantitative information concerning steric effects of simple alkyl groups is derived from the extensive kinetic correlations obtained from studies of the acid-catalyzed hydrolysis of esters.[1] The reaction is believed to involve conversion of the trigonal ester reactant to a tetrahedral hydrated species which lies close to the activated complex on the reaction coordinate. Since the polar effects of the substituents are known to be minimal in this reaction, the differences in rate correspond to differences in steric interaction between the alkyl group and the trigonal center of the reactant vs. the tetrahedral center of the activated complex (eq 1).

Taft's E_s values are the logarithms of the relative rate ratios referred to methyl as the standard group, and are proportional to the free-energy changes attending substitution. Other steric substituent parameters have been developed which correct this basic scheme for additional effects on the relative rates (i.e., hyperconjugation),[2] but most of the approaches agree on the relative ordering of the steric effects of simple alkyl substituents.

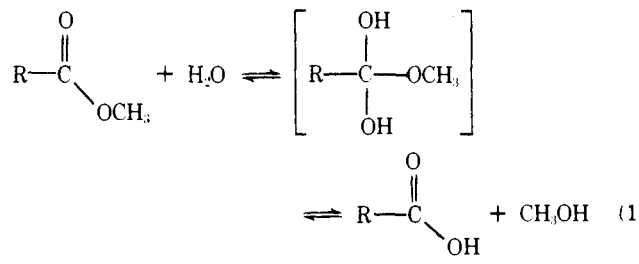

We wished to determine the enthalpy component of the steric interaction of an alkyl group with a trigonal vs. tetrahedral center and thus were led to examine the enthalpies of hydrolysis of substituted dimethyl ketals (eq 2). Here the

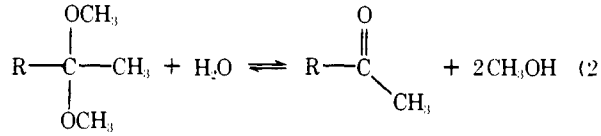

structures of the species taking part in the steric interactions are well defined, and the hydrolysis is considered to be a reasonable model for the activation process depicted in eq 1.

0002-7863/79/1501-5512$01.00/0